Nanoscale

PAPER

View Article Online
View Journal | View Issue

Cite this: *Nanoscale*, 2025, **17**, 4636

How tailor-made copolymers can control the structure and properties of hybrid nanomaterials: the case of polyionic complexes†

Liming Peng,‡[a] Maksym Odnoroh,[a] Mathias Destarac,[a] Yannick Coppel,[b] Céline Delmas,[c] Florence Benoit-Marquié,[a] Christophe Mingotaud[a] and Jean-Daniel Marty *[a]

Received 20th October 2024,
Accepted 7th January 2025

DOI: 10.1039/d4nr04332d

rsc.li/nanoscale

Hybrid polyionic complexes (HPICs) are colloidal structures with a charged core rich in metal ions and a neutral hydrophilic corona. Their properties, whether as reservoirs or catalysts, depend on the accessibility and environment of the metal ions. This study demonstrates that modifying the coordination sphere of these ions can tune the properties of HPICs by altering the composition of the complexing block or varying formulation conditions. Hence, double hydrophilic block copolymers were synthesized using RAFT polymerization, with polyethylene glycol as the neutral block and different ratios of acrylic acid (AA) and vinylphosphonic acid (VPA) as the functional block and further complexed with Fe(III) ions. The resulting iron-based HPICs with higher VPA content were more stable at low pH due to stronger VPA-iron interactions, but their catalytic efficiency in the photo-Fenton process decreased at higher pH. In nanoparticle synthesis, polymers with higher VPA content produced smaller, less-defined Prussian blue nanoparticles, while a 50/50 AA/VPA ratio resulted in uniform nanoparticles and optimal reactivity. Multivariate analysis revealed that not only composition but also local structural organization impacts HPIC properties, influenced by changes in the complexing block structure (*e.g.*, statistical, block) or formulation conditions.

Introduction

Thanks to advances in controlling their synthesis, polymers have become essential building blocks in numerous formulations today. Various parameters, including their molar mass, chemical composition, tacticity, microstructure (statistical, block, alternating, gradient), or architecture (linear, branched) can be adjusted.[1–5] This structural modularity enables tailored adaptation to specific applications by finely tuning their intrinsic properties such as solubility, viscosity, *etc.*[6–9] In addition to these macromolecular parameters, polymer-based formulations are also sensitive to kinetic factors.[10,11] Surfactant micelles are dynamic structures that naturally break apart in aqueous solution below a critical micellar concentration.[12–14] In contrast, polymer micelles retain their stability even under thermodynamically unfavorable conditions. This additional characteristic makes them ideal materials for constructing vectors used in nanomedicine applications.[15–18]

In this context, double hydrophilic block copolymers (DHBCs) have garnered significant attention in recent years, with extensive research and study focused on their properties and applications.[19–24] Due to their structure, DHBCs are perfectly soluble in aqueous solutions. Aggregation of these polymers in such environments can be triggered through various mechanisms.[19,25] For instance, if one of the blocks is responsive to an external stimulus such as temperature or pH, applying this stimulus can alter the solubility of that block, thereby inducing self-aggregation in solution.[26–31] Another method to prompt aggregation is by adding an external compound that interacts with one of the two blocks, facilitating the structuring of the polymers.[32] Research by Kataoka and colleagues has highlighted the formation of polyionic complexes vector through the addition of active ingredients that interact with a functional block such as a charged block.[33] More recently, hybrid polyionic complexes, often referred to as HPICs, have been obtained by combining a complexing polymer such as poly(ethylene glycol)-*b*-poly(acrylic acid) (PEG-*b*-PAA) with a divalent or trivalent ion. These hybrid complexes have been

[a]*Laboratoire Softmat, Université de Toulouse, CNRS UMR 5623, 118 route de Narbonne, 31062 Toulouse Cedex 9, France. E-mail: jean-daniel.marty@univ-tlse3.fr*
[b]*Laboratoire de Chimie de Coordination, Université de Toulouse, CNRS UPR 8241, 205 route de Narbonne, 31062 Toulouse, France*
[c]*MIAT UR 875, INRAE, Université de Toulouse, F-31326 Castanet-Tolosan, France*
†Electronic supplementary information (ESI) available. See DOI: https://doi.org/10.1039/d4nr04332d
‡Current address: School of Chemistry, Chemical Engineering, and Materials, Jining University, Qufu, Shandong 273155, China.

applied in various fields, including catalysis,[34–36] medical imaging,[37–42] or as templates for the synthesis of inorganic materials.[41,43–46]

The strength of interactions within these HPICs is a key element for controlling the properties of the final object. For a given multivalent ion, it depends primarily on the nature of complexing function but also on external conditions such as pH.[19] For example, in HPICs based on the complexation of gadolinium with DHBCs, whereas ionizing block based on carboxylic acid were destabilized below a pH of 4, those based on stronger phosphonic[47,48] or bisphosphonic[49] acid remained stable at pH values lower than 2.

This article aims to address several questions to decipher how it is possible to tune the properties of HPICs by adjusting the coordination sphere of their metal ions. Modulation will be achieved either by modifying the composition of the complexing block or by varying the formulation conditions. To investigate these questions, DHBCs comprising PEG as the neutral block and a combination of AA and VPA units as the charged block (with a molar percentage of VPA ranging from 0 to 100) were synthesized with varying microstructures and compositions. Fe(III) ions were selected to form HPICs as illustrated in Scheme 1. In addition (*vide infra*) different formulation methods will be used to change local organization within HPICs while keeping the composition constant. The catalytic properties and the capacity of the different solutions of HPICs to act as reservoirs for the formation of Prussian blue nanoparticles were then examined.

Experimental section

Chemical products

$FeCl_3$,6·H_2O, $K_4Fe(CN)_6$,3·H_2O, vinylphosphonic acid (VPA, 97%), acrylic acid (AA, 99%), 2,2′-azobis(iso-butyramidine) dihydrochloride (AIBA, 97%), 1,10-phenanthroline, NH_2OH·HCl, H_2O_2, NH_4OH, methyl sulfone, sodium acetate (AcONa), Acid Black 1 (noted AB1), NaOH and 1 mol L^{-1} HCl are all from Sigma-Aldrich. Water was purified through a filter and ion exchange resin by using a Purite device (resistivity 18.2 MΩ cm).

Synthesis of PEG-*b*-P(AA_x-*st*-VPA_{1-x}) copolymers

The synthesis method of the different DHBCs was conducted as described in previous reports.[48]

Preparation of HPICs-Fe solutions

HPICs made of a statistical copolymer (PEG-*b*-P(AA_x-*st*-VPA_{1-x})) (see Method 3 in Scheme 2, main text). HPICs formation was investigated by maintaining a constant concentration of $PEG_{2.2k}$-*b*-P(AA_x-*stat*-VPA_{1-x})$_{0.9-1.2k}$ (0.1 wt%) while varying the amount of $FeCl_3$ to achieve a range of *R* values, $R = 3\cdot[Fe^{3+}]/[(AA + VPA)^-]$, from 0 to 3. The values of *x* were set at 100, 75, 50, 25, and 0%. The mixtures of iron solutions and copolymer solutions were stirred for one hour before being used. The resulting HPICs, synthesized with statistical copolymers, are denoted as **ST-HPICs**. When *x* takes the maximum value (1), the copolymer is PEG-PAA, and the resulting sample is noted HPICs-PAA. The HPICs-PVPA sample was synthesized with the copolymer PEG-PVPA. pH of HPICs-Fe samples was changed, if needed, by adding HCl solution (0.1 mol L^{-1}) or NaOH solution (0.1 mol L^{-1}).

The samples resulting from the mixing of HPIC solutions (see Method 3 in Scheme 2, main text) are denoted **MH-HPICs**. They are made by combining two HPIC solutions with an identical *R* value of unity, where one solution contains HPICs-PAA and the other contains HPICs-PVPA. By adjusting the volumes of these two mixed solutions, it is possible to set the final and macroscopic molar ratio between AA and VPA (75AA/25VPA, 50AA/50VPA, and 25AA/75VPA).

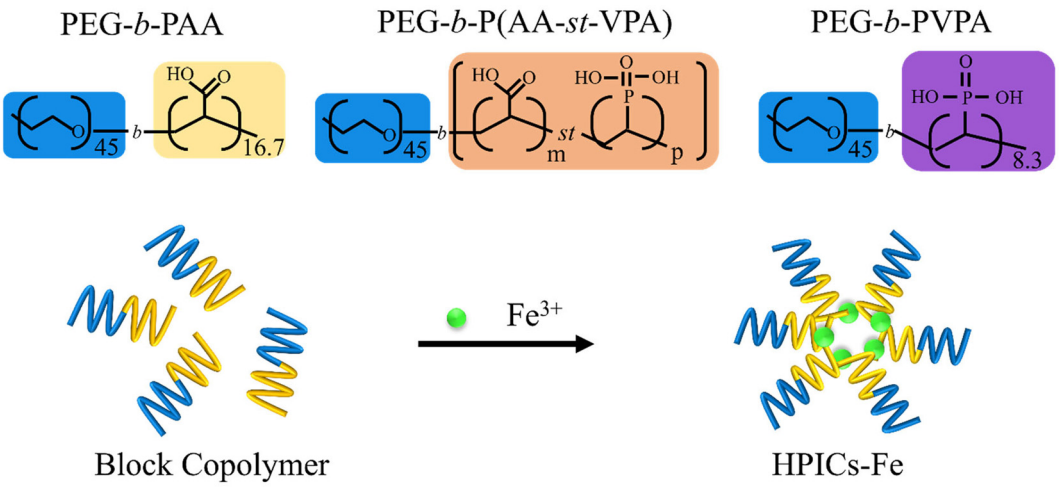

Scheme 1 Chemical structure of the DHBCs comprising acrylic acid and vinylphosphonic acid as complexing units and schematic representation of HPICs formation by using Fe^{3+} to different DHBCs. The indicated values represent the number of repetition units and for PEG_{45}-*b*-P(AA_m-stat-VPA_n), *m*/*n* takes the different values 9.3/3.6; 5.6/5.2; 2.5/5.3 (see also Table 2).

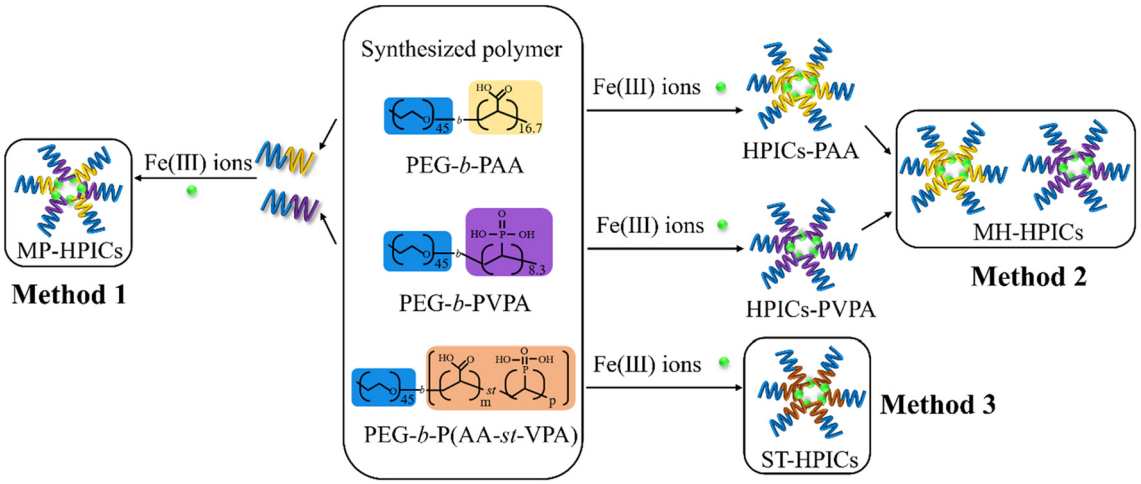

Scheme 2 Schematic diagram of HPICs samples obtained using three different methods to mix DHBCs containing acrylic acid and vinylphosphonic acid as complexing units. Method 1: HPICs formed from a mixture of polymers (samples denoted **MP-HPICs**). Method 2: mixing of pristine HPICs (samples denoted **MH-HPICs**). Method 3: HPICs formed from a block-Statistical copolymer (samples denoted **ST-HPICs**).

The samples resulting from the mixing of polymers before the formation of HPICs (see Method 1 in Scheme 2, main text) are denoted **MP-HPICs**. Firstly, the synthesized $PEG_{2.2k}$-*b*-$PAA_{1.2k}$ and $PEG_{2.2k}$-*b*-$PVPA_{0.9k}$ block copolymers were mixed at different molar ratios (75AA/25VPA, 50AA/50VPA, and 25AA/75VPA). Subsequently, the HPICs samples were synthesized with a R value of unity.

Preparation of HPICs samples for NMR studies

PEG-*b*-PAA (67.3 mg mL^{-1}), PEG-*b*-PVPA (34.2 mg mL^{-1}), $Ga(NO_3)_3$ (38.8 mg mL^{-1}) and methyl sulfone (6 mg mL^{-1}) solutions were prepared using D_2O as solvent. Mixing of these 3 solutions was done according to the proportions in the Table 1.

Colorimetric titration

Uncomplexed Fe^{3+} ions were determined by colorimetric method. First, a standard measurement was performed. 0.2 mL of a low pH (1 or 3) Fe^{3+} solution (0.5 mmol L^{-1}) was added to 2 mL of a NaOAc solution (100 mmol L^{-1}). Then, 0.03 mL of a $NH_2OH{\cdot}HCl$ solution (60 mmol L^{-1}) was mixed with the previous solution to reduce ferric ions into ferrous ions. Finally, 0.07 mL of a 1,10-phenanthroline solution (10 mmol L^{-1}) is added to the mixture. The absorbance at 510 nm of the final standard solution is measured by UV-vis spectrum after standing for 10 min. Dialysis membranes are used to filter out undissociated HPICs to avoid affecting the results.

Characterization

UV/vis spectra were recorded with a Hewlett Packard 8452A or an Analytik Jena Specord 600 spectrometer at room temperature, with 10 mm path length quartz cuvettes. Dynamic light scattering (DLS) characterization was performed on a Zetasizer Nano-ZS (Malvern Instruments Ltd, UK) with a 4 mW He–Ne laser (λ = 633 nm, light scattering measured at 173°). The correlation functions were analyzed using the cumulant method to get the Z-average diameter of the colloidal particles. Simultaneously, the NNLS (Non-Negative Least Squares) general-purpose method was employed to estimate the distribution in size of the colloids. Three separate runs were made to calculate standard deviations. Transmission electron microscopy (TEM, MET Hitachi HT7700, accelerating voltage of 80 kV) was used to characterize the morphology and size of

Table 1 Volumes of the various stock solutions added for the preparation of the different samples studied by NMR

Samples	PEG-*b*-PAA (μL)	D_2O (μL)	Ga^{3+} (μL)	PEG-*b*-PVPA (μL)
(1) Pure PEG-*b*-PAA	40.5	660	—	—
(2) PEG-*b*-PAA + Ga (R = 1.0)	40.5	630	30.1	—
(3) Pure PEG-*b*-PVPA	—	549	—	151
(4) PEG-*b*-PVPA + Ga (R = 1.0)	—	518	30.1	151
(5) (PEG-*b*-PAA + Ga, R = 1.0) + 25% PEG-*b*-PAA	40.5	590	30.1	39
(6) (PEG-*b*-PAA + Ga, R = 1.0) + 50% PEG-*b*-PAA	40.5	551	30.1	78
(7) (PEG-*b*-PAA + Ga, R = 1.0) + 100% PEG-*b*-PAA	40.5	479	30.1	151

25%, 50% and 100% refer to the molar amount of added PEG-*b*-PVPA compared to PEG-*b*-PAA.

HPICs and Prussian blue particles. Their solutions were dried on copper grids with a mesh size of 200. Statistical analysis of sizes was carried out using Nano Measurer software. The size distribution statistics were obtained from multiple TEM images captured from the same sample. Nuclear Magnetic Resonance (NMR) experiments were conducted in D_2O at 298 K using a Bruker Avance 600 NEO spectrometer equipped with a 5 mm triple resonance inverse *Z*-gradient probe (TBI ^{1}H, BB). A relaxation delay of 15 s was employed to ensure the acquisition of accurate ^{1}H integration data. The T_1 spin–lattice relaxation times were determined utilizing the inversion recovery method.

Photo-Fenton experiments

Photo-Fenton degradation of Acid Black 1 (AB1) was chosen to characterize the catalytic activity of HPICs. The ratio between the catalyst (HPICs with R = 1.0), the model pollutant AB1 (5×10^{-4} mol L^{-1}) and H_2O_2 (4×10^{-2} mol L^{-1}) in 2 mL mixed solution is 1 : 1 : 40. HPICs solutions include HPICs-PAA, **ST-HPICs** (75AA/25VPA, 50AA/50VPA, and 25AA/75VPA), **MH-HPICs** (75AA/25VPA, 50AA/50VPA, 25AA/75VPA), **MP-HPICs** (75AA/25VPA, 50AA/50VPA, and 25AA/75VPA) and HPICs-PVPA. The reaction was initiated by white irradiation with a SCHOTT KLC 1500 LCD lamp (600 lumens). The real-time concentration of AB1 was tracked by ultraviolet-visible absorption at 618 nm. The degradation efficiency of AB1 by the HPICs catalyst is:

$$\text{AB1 degradation level } (\%) = [1\ (C_t/C_0)] \times 100\%$$

C_0 and C_t are the concentrations of acid black at the initial time and reaction time t, respectively.

Prussian blue synthesis experiments

Different types of HPIC solutions serve as pre-organized systems for the controlled synthesis of Prussian blue nanostructures after addition of potassium ferrocyanide. The above different HPICs with a R value of 1.0, including HPICs-PAA, **ST-HPICs** (75AA/25VPA, 50AA/50VPA, and 25AA/75VPA), **MH-HPICs** (75AA/25VPA, 50AA/50VPA, 25AA/75VPA), **MP-HPICs** (75AA/25VPA, 50AA/50VPA, and 25AA/75VPA), HPICs-PVPA, were sequentially tested as a preorganized system. The ferrocyanide salt solution was mixed with the HPIC solutions according to the specified ratio ($[Fe^{3+}]/[Fe(CN)_6^{4-}]$ = 4/3). Real-time monitoring of Prussian blue formation was done by UV-vis spectroscopy.

Kinetics analysis

A very straightforward and phenomenological kinetic model was used to fit the absorption *versus* time curves recorded during the formation of Prussian blue. Briefly, our model proposes that $Fe(CN)_6^{4-}$ initiates the formation to a product A with a pseudo first-order law and a constant k_1. This product is characterized by a specific absorbance Abs_0. Product A can further react to form a second product B, characterized by an absorbance $\alpha \cdot Abs_0$ where α is a constant. We assumed that this secondary reaction also follows a pseudo first order law with a constant k_2. Then, the absorbance of the solution will be given by the equation:

$$Abs = \frac{Abs_0}{(k_1 - k_2)} \cdot \left[\alpha \cdot (k_1 - k_2) - (k_1 - \alpha \cdot k_2) \cdot e^{-k_1 \cdot t} + (1 - \alpha) \cdot k_1 \cdot e^{-k_2 \cdot t}\right]$$

The proposed model fits well the experimental absorption measured during the generation of Prussian blue nanoparticles.

Results and discussion

Formation and characterization of HPICs

A series of five $PEG_{2.2k}$-*b*-$P(AA_x$-*st*-$VPA_y)_{1k}$ copolymers were synthesized for various molar ratios of AA/VPA ranging from 100/0% to 0/100%. An aqueous reversible addition–fragmentation chain transfer (RAFT) polymerization of AA with VPA was performed for that in the presence of a xanthate-based $PEG_{2.2k}$ macro-RAFT agent. Owing to the disparate reactivities of AA and VPA in radical copolymerization, a semi-batch polymerization in which a solution of AA in water was added dropwise for 6 h to a solution of $PEG_{2.2k}$-XA, VPA, and AIBA (2,2′-azobis (isobutyramide) dihydrochloride) in water was carried out as previously described, in order to avoid a compositional drift and ensure a statistical distribution of AA and VPA.[48] The characteristics of these different purified polymers are summarized in Table 2. These polymers were subsequently used to obtain HPIC structures by maintaining their concentration constant (0.1 wt%) while varying the amount of $FeCl_3$ to achieve a range of R values, $R = 3 \cdot [Fe^{3+}]/[(AA + VPA)]$, from 0 to 3.

These colloids are based on the use of statistical copolymers to form HPICs structures and will be noted as HPICs-P(AA_x-*st*-VPA_{1-x}) or **ST-HPICs** in the followings. In aqueous solution and in the absence of polymer, Fe^{3+} ions have a limited pH stability range: above pH 2.5, the $Fe(OH)^{2+}_{aq}$, $Fe(OH)_2{}^{+}_{aq}$ and $Fe_2(OH)_2{}^{4+}_{aq}$ species are predominant, while above pH 5 the formation of $Fe(OH)_{3(s)}$ precipitates is observed.[35,50–52] Adding DHBCs to a solution of Fe^{3+} ions prevents the formation of $Fe(OH)_{3(s)}$ precipitates up to pH 7, as long as the ratio R between the positive charges of the iron ions and the negative ones due to the ionized or ionizable carboxylic or phosphonic functions remained below 1.

To evaluate the impact of the interactions between Fe(III) ions and AA or VPA units on the colloidal properties of the studied system, HPICs solutions obtained at various R ratio with the different synthesized copolymers were further analyzed by DLS. The solutions of PEG-*b*-$P(AA_x$-*st*-$VPA_{1-x})$ block copolymers are characterized by a very weak scattered intensity and the corresponding correlograms are associated with a *Z*-average size (diameter) above 180 nm (Fig. S1†). This was likely caused by the presence of poorly defined self-associations of the copolymers through hydrogen bonding.[39] The addition of iron ions leads to an increase in scattered intensity for ratios up to R = 1 after which the measured intensity remains constant. Simultaneously, the analysis of correlo-

Table 2 Main characteristics of the synthesized polymers

Polymer	Conversion AA[a]/VPA,[b] %	Ratio AA/VPA, molar,[c] %	$M_{n\ (NMR)}$,[d] kg mol^{-1}	$M_{n\ (SEC)}$,[e] kg mol^{-1}	$Đ^e$ (M_w/M_n)	dn/dc,[f] mL g^{-1}
PEG_{45}-*b*-$PAA_{16.7}$	99/—	100/0	3.4	5.3	1.05	0.147
PEG_{45}-*b*-P($AA_{9.3}$-*stat*-$VPA_{3.6}$)	99/58	72/28	3.3	4.9	1.10	0.146
PEG_{45}-*b*-P($AA_{5.6}$-*stat*-$VPA_{5.2}$)	99/46	52/48	3.2	3.2	1.30	0.146
PEG_{45}-*b*-P($AA_{2.5}$-*stat*-$VPA_{5.3}$)	99/34	32/68	3.0	2.8	1.41	0.145
PEG_{45}-*b*-$PVPA_{8.3}$	—/47	0/100	3.1	4.4	1.26	0.144

[a] Determined by ^{1}H NMR. [b] Determined by ^{31}P NMR. [c] Calculated by theoretical molar masses. [d] Calculated by formula $M_n = (m_{AA}\cdot conv._{AA} + m_{VPA}\cdot conv._{VPA})\cdot M_{n\ PEG\text{-}XA}/m_{PEG\text{-}XA} + M_{n\ PEG\text{-}XA}$. [e] Determined by SEC-RI-MALS. [f] Measured by differential refractometer. The values given are subscript correspond to the average number of repeat unit in each block: for all polymers, neutral PEG block has an average molar mass equal to 2000 g mol^{-1}, whereas the one of complexing block is equal to 1000 g mol^{-1}. The indicated values represent the number of repeat units.

grams reveals the progressive disappearance of large, poorly defined polymer aggregates in favor of monodisperse with comparable sizes ranging from 20 to 30 nm objects (Fig. S1 and Table S1†). These colloids have a core–shell structure with the core being rich in iron ion species as evidenced also on TEM images (Fig. S2†).[39] In the following sections, only systems with a R ratio equal to 1 are considered. It should be noted that the formation of objects is very rapid, with the complexation process completed within a few seconds.[34]

If the colloidal structures obtained with the various polymers are roughly the same, their chemical stability is dramatically different as illustrated in Fig. 1. At pH above 3, complexes formed by Fe(III) ions with PEG-*b*-PAA (named HPICs-PAA) exhibit an absorbance spectrum with a distinct peak at 350 nm, indicating the primarily formation of iron hydroxide complexes (Fig. 1a and c).[53] Complexation with carboxylate ions does not prevent the formation of hydroxylated iron species, although it does inhibit the formation of precipitates in solution. Notably, this peak vanishes when the carboxylic acid functions are substituted with phosphonic acid functions in PEG-*b*-PVPA, resulting in a completely colorless solution appearing at pH 3 (Fig. 1b and c). This observation suggests a stronger interaction between iron ions and the phosphonic acid groups, compared to the carboxylic acid groups. Furthermore, for HPICs-PAA system, lowering the pH below 3 leads to a significant increase in the measured Z average sizes. This increase is associated with the protonation of carboxylate groups, which induces a progressive decomplexation of iron ions and, consequently, the disappearance of the HPIC structures. No such behavior is observed for HPICs based on PEG-*b*-PVPA copolymers (named HPICs-PVPA, Fig. 1d). This difference is partly attributed to the lower pK_a value of VPA compared to AA (2.7 and 4.5, respectively), which reduces the competition between complexation and protonation.

VPA and AA have therefore different affinities for Fe(III) ions. Thus, integrating VPA into the polymer structure enhances the interaction between the polymers and Fe(III) ions. Consequently, for all ST-HPICs incorporating VPA, the presence of VPA limits the iron speciation (Fig. S3†) and prevents decomplexation phenomena at low pH, preserving the HPIC structure even at pH 1 (Fig. S4†).

Effect of VPA content on catalytic properties in ST-HPICs

To assess the impact of incorporating VPA on the properties of HPIC structures, their ability to catalyze the degradation of a model pollutant (naphthol blue black, AB1) using a photo-Fenton process at different pH levels was investigated (Fig. 2). For consistency and comparative purposes, experimental conditions similar to those previously described in literature are chosen,[34–36] with a molar ratio Fe(III) ions : AB1 : hydrogen peroxide set to 1 : 1 : 40. HPICs samples with R = 1 was selected to ensure no uncomplexed Fe(III) was present in solution.

The degradation of AB1 was followed by UV-visible absorption under light irradiation. As example, considering HPICs-PAA at pH 3 as catalyst, the evolution of the UV-Vis spectrum of the solution with time can be analyzed by a pseudo-first-order kinetic model (Fig. 2a).[54] The conversion of the reaction after 2 h was 74%, which is slightly lower compared to the 99% conversion achieved with pure Fe(III) at this pH. When examining the conversion evolution at pH 3 relative to the VPA content, a nearly linear dependency of conversion on the molar content of VPA (Fig. 2b) was obtained. A higher VPA content significantly decreases the observed conversion rate. This effect is attributed to the strong interaction between VPA and iron ions, which alters the complexation sphere and modifies the redox potentials, subsequently affecting the production of hydroxyl radicals. The impact of pH on these catalytic systems was then assessed (Fig. 2c and Fig. S5†). For the HPICs-PAA system, catalytic activity peaks at pH 3.

At pH below 3, a decrease of conversion level was observed. This is attributed to the high concentration of protons in solution, which reduces the rates of generation of ferrous ions and hydroxyl radicals, consequently impacting the degradation of AB1, as described in the literature.[55] At pH above 3, the catalytic activity diminishes, as anticipated in this process due to the formation of less reactive iron species.[56] For such pH, the inclusion of VPA into the HPIC structures leads to a significant decrease in conversion rates. While VPA prevents the formation of hydroxylated forms of iron at these pHs, its presence still diminishes the capacity of the structures to generate reactive oxygen species. At pH below 3, the presence of VPA induced significantly different behaviors compared to the HPICS-PAA system, particularly when the VPA content exceeds 25%. In this case, the measured conversion increases as the

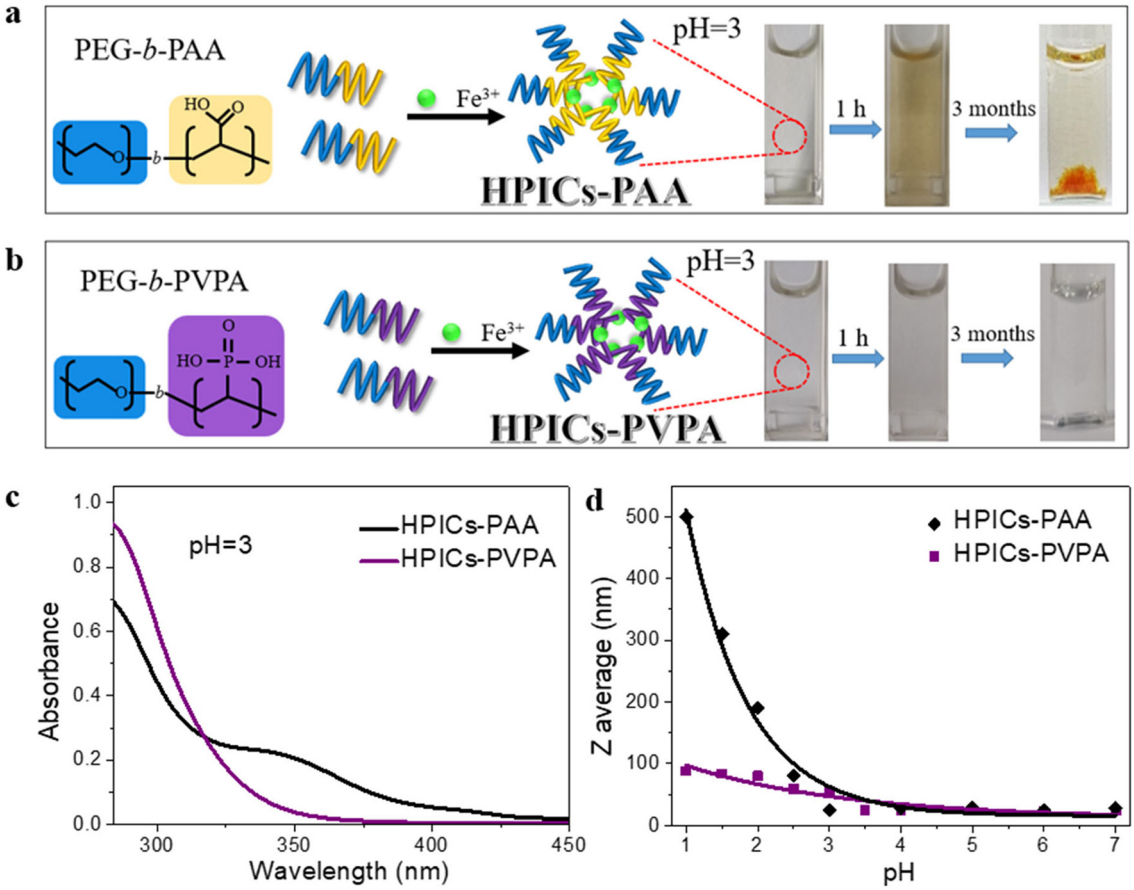

Fig. 1 (a) Formation of HPICs-PAA and (b) HPICs-PVPA. Aspect of their solutions at different time (0 h, 1 h, 3 months). R = 1.0. Concentration of Fe is 1.8 × 10^{-3} mol L^{-1} and pH = 3. (c) UV-Vis spectra of HPICs-PAA and HPICs-PVPA solutions (after 1 h). (d) Z-Average diameter of the colloids in solution depending on pH and polymer structure.

pH decreases. The presence of Fe(III) ions within the HPIC structures maintains their reactivity even at low pH. This effect is particularly noticeable for a AA/VPA composition of 50/50, which appears to offer the best compromise between stability and accessibility of iron(III) ions (Fig. 2d).

Effect of VPA content on the formation of Prussian blue nanoparticles in ST-HPICs

Hybrid polyionic complexes can also act as a chemical reservoir for Fe(III) ions from which the availability of complexed ions can be easily tuned through a precise pH control of the solution.[43] This property has recently been exploited to enable the formation of Prussian blue (PB) nanostructures with different sizes and compositions, through the addition of $K_4Fe(CN)_6$ to HPICs, as illustrated in Fig. 3a.[43] The results discussed above demonstrated that the insertion of VPA within HPICs structure induced a modification of the complexation sphere of Fe(III) at a chosen pH. This modification also is likely to impact the ability of HPICs to act as a reservoir for the synthesis of PB nanoparticles. To study their formation and associated kinetic, UV-visible spectroscopy was further used. At pH 6, for a chosen concentration of Fe(III) ions, the maximum absorbance measured after 2 hours decreases proportionally to the VPA content in the copolymer (Fig. 3b).

The formation kinetics are represented in Fig. 3c. These spectroscopic data were fitted and analyzed using a phenomenological model involving the formation of PB either with two characteristic reaction rate k_1 and k_2 (see kinetic model in ESI†). As seen in Fig. 3d and Fig. S6,† the evolution of the kinetic constant k_2 remains relatively constant or exhibits a linear dependency *versus* the composition of the copolymer. In contrast, the k_1 constant is distinctly non-linear, displaying a maximum around the composition containing 50% VPA. This feature is specific to the **ST-HPICs** as demonstrated below. The size and morphology of the nanoparticles were determined from TEM pictures, as illustrated in Fig. 3e. The increase in the VPA content induces both a decrease in the measured average size from 51 ± 10 nm for 0% VPA to 18 ± 4 nm for 100% VPA (Fig. S6†) and the formation of less well-defined cubic-shaped particles. Indeed, the percentage of nanocubes among all the PB particles on the TEM pictures decreases as the percentage of VPA increases (see Fig. 3e). This may be due to differences in interaction between the copolymers and the surface of the PB nanoparticles.

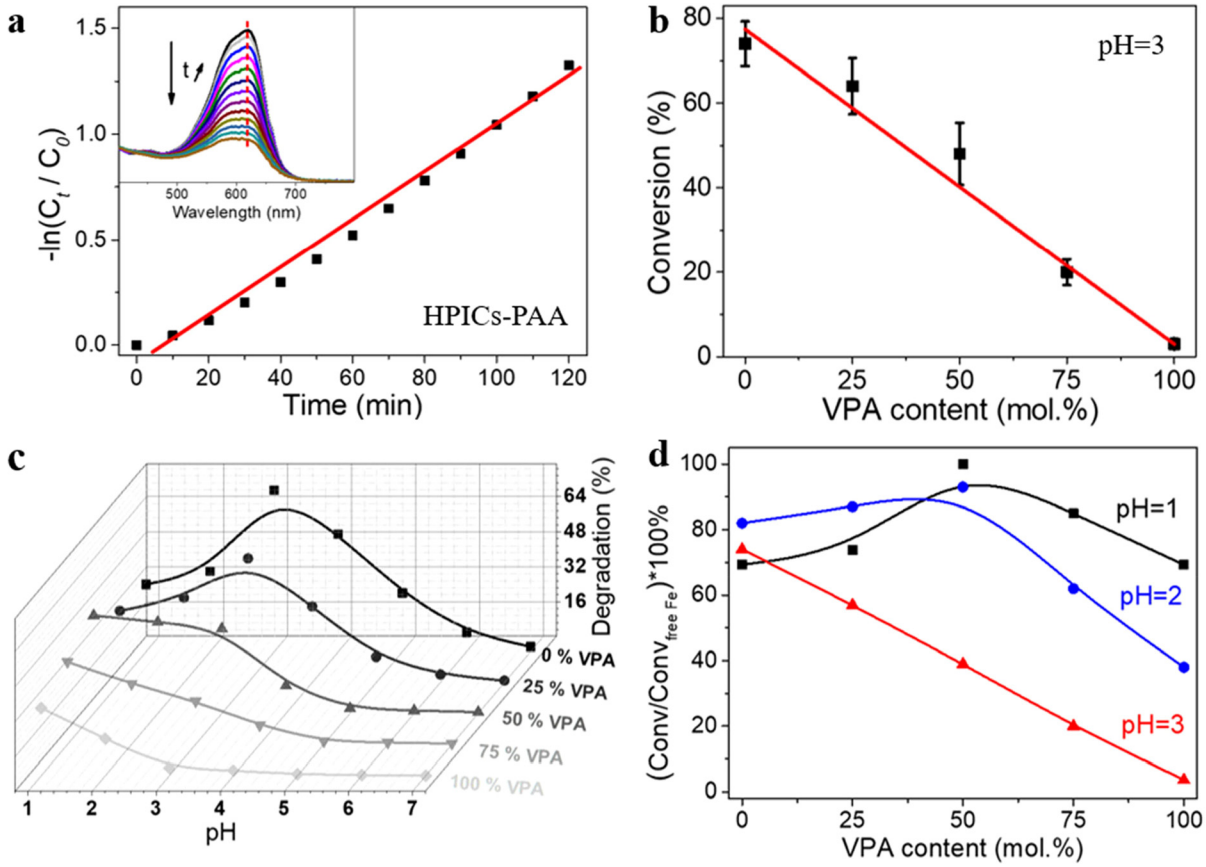

Fig. 2 (a) Real-time photo-Fenton degradation effect of AB1 by HPICs-PAA at pH = 3 following the decrease of the absorbance at 618 nm. Inset: evolution of AB1's UV-Vis spectrum with reaction time. Irradiation started at t = 0 min. (b) Comparison of photo-Fenton degradation effects of **ST-HPICs** with different VPA contents at pH = 3 and a reaction time of 2 h. (c) Photo-Fenton degradation effect of HPICs-Fe on AB1 for different VPA contents and different pH conditions, reaction time: 2 h. (d) Comparison of the photo-Fenton degradation effects of HPICs with different VPA contents at pH = 1, 2 or 3. $Conv/Conv_{free\ Fe}$ is the ratio of the degradation effect of HPICs-Fe to free Fe^{3+}. Reaction conditions: **ST-HPICs**-Fe, R = 1.0, $[Fe^{3+}] = 1.3 \times 10^{-5}$ mol L^{-1}, [AB1] = 2.2×10^{-5} mol L^{-1}, $[H_2O_2] = 1.5 \times 10^{-3}$ mol L^{-1}, reaction time: 2 h.

Effect of colloid structure on reactivity

These first examples highlighted the crucial role of the composition on the properties of studied colloid, indicating that the modification of the complexation sphere is a key factor explaining the observed properties. But can the polymer microstructure, aside from its composition, play a role in the environment of the metal centers and, consequently, on the observed properties?

To assess this possibility, two additional colloidal solutions were prepared using different strategies while maintaining a constant AA/VPA ratio as illustrated in Scheme 2. The first method (Method 1) involves pre-mixing the two copolymers, PEG-*b*-PAA and PEG-*b*-PVA, with the chosen AA/VPA ratio, followed by the addition of Fe(III) ions to presumably form mixed HPICs (noted HPICs-(PAA_x + $PVPA_{1-x}$) or **MP-HPICs**). The second method (Method 2) entails the direct mixture of preformed HPICs-PAA and HPICs-PVPA (noted $(HPICs\text{-}PAA)_x$ + $(HPICs\text{-}PVPA)_{1-x}$ or **MH-HPICs**). The properties of these diverse different colloidal solutions (**ST-HPICs**, **MP-HPICs** or **MH-HPICs**), which differ in composition or structure, were then compared. In particular, the availability and accessibility of ions trapped in the HPICs were evaluated through their catalytic properties and the formation Prussian blue as previously described for **ST-HPIC** solutions.

Regardless of the method used to achieve a given AA/VPA ratio, the average size of the final objects in solution (see Table 3) falls within the range of 20–30 nm in diameter, as previously described for the **ST-HPICs**. A closer examination of these data reveals that the sizes of **MP-HPICs** and **MH-HPICs** are very similar, with the main size differences observed in the **ST-HPICs**.

The study of the catalytic efficiency of different structures for the degradation of AB1 is illustrated in Fig. 4a for a composition of 50/50 in AA and VPA. For all pH values, the organization resulting from the use of statistical polymers leads to optimal reactivity, while the **MP-HPICs** system exhibit the lowest reactivity. Moreover, the method used to achieve a given AA/VPA composition also significantly impacts the formation of Prussian blue nanoparticles. Regarding their formation

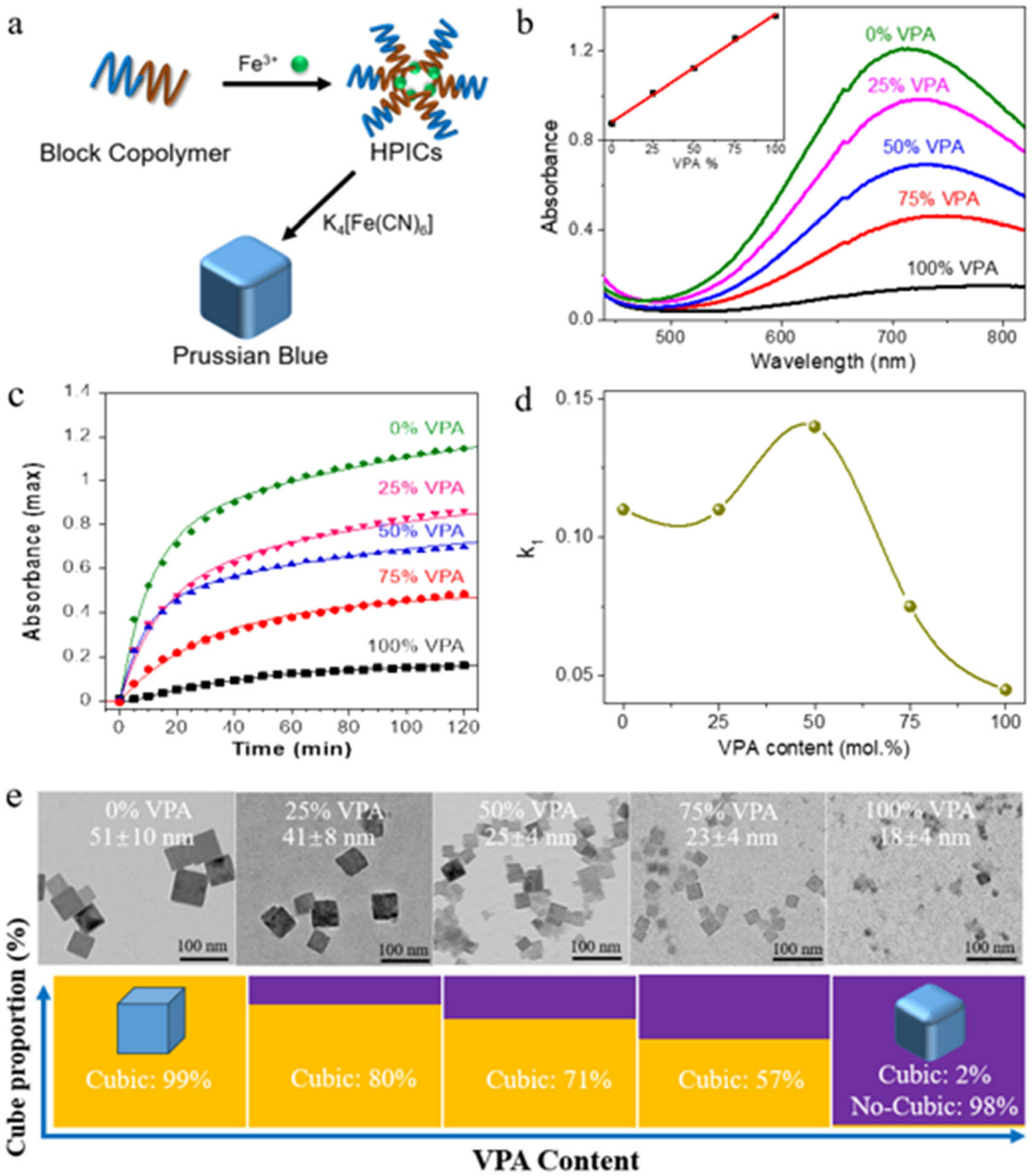

Fig. 3 Formation of Prussian blue nanoparticles starting from **ST-HPICs** systems: effect of VPA content. (a) Schematic formation of Prussian blue nanoparticles (b) Absorbance spectra and evolution of the maximum absorbance (inset) for solutions with different VPA content. The spectra were recorded 2 h after addition of $K_4Fe(CN)_6$. (c) Evolution of the maximum absorbance as a function of time. (d) Evolution of kinetic parameter k_1 as a function of VPA content using **ST-HPICs** as a pre-organized system. (e) Evolution of the morphology of Prussian blue nanoparticles based on **ST-HPICs** with different VPA content studied by TEM and corresponding fraction of cubic morphology as a function of VPA content. The size distribution was obtained by analyzing manually more than 100 particles from 3 to 5 different TEM images for each composition.

Table 3 Comparison of hydrodynamic dimensions (*Z* average diameter) of **ST-HPICs**, **MP-HPICs** and **MH-HPICs**

Composition (AA/VPA)	ST-HPICs size (nm)	MP-HPICs size (nm)	MH-HPICs size (nm)
100/0	24 ± 0.7	24 ± 3.1	24 ± 3.1
75/25	16 ± 8.0	27 ± 4.6	29 ± 3.7
50/50	36 ± 18	21 ± 2.3	22 ± 3.3
25/75	30 ± 18	23 ± 2.8	25 ± 2.7
0/100	20 ± 3.6	20 ± 3.2	20 ± 3.2

kinetics, no substantial differences were observed in the k_2 constant among **ST-HPICs**, **MH-HPICs** and **MP-HPICs** (Fig. S7–S9†). In contrast, the non-linear dependency of k_1 on the AA/VPA ratio observed for **ST-HPICs** (see above) is not found in the **MH-HPICs** or **MP-HPICs** colloidal systems. For these two systems, the k_1 values are very similar and exhibit a simple linear dependency with the AA/VPA composition (Fig. 4b). For all three types of organizations, the size of Prussian blue gradually decreases with increasing VPA content (Fig. S10†). In

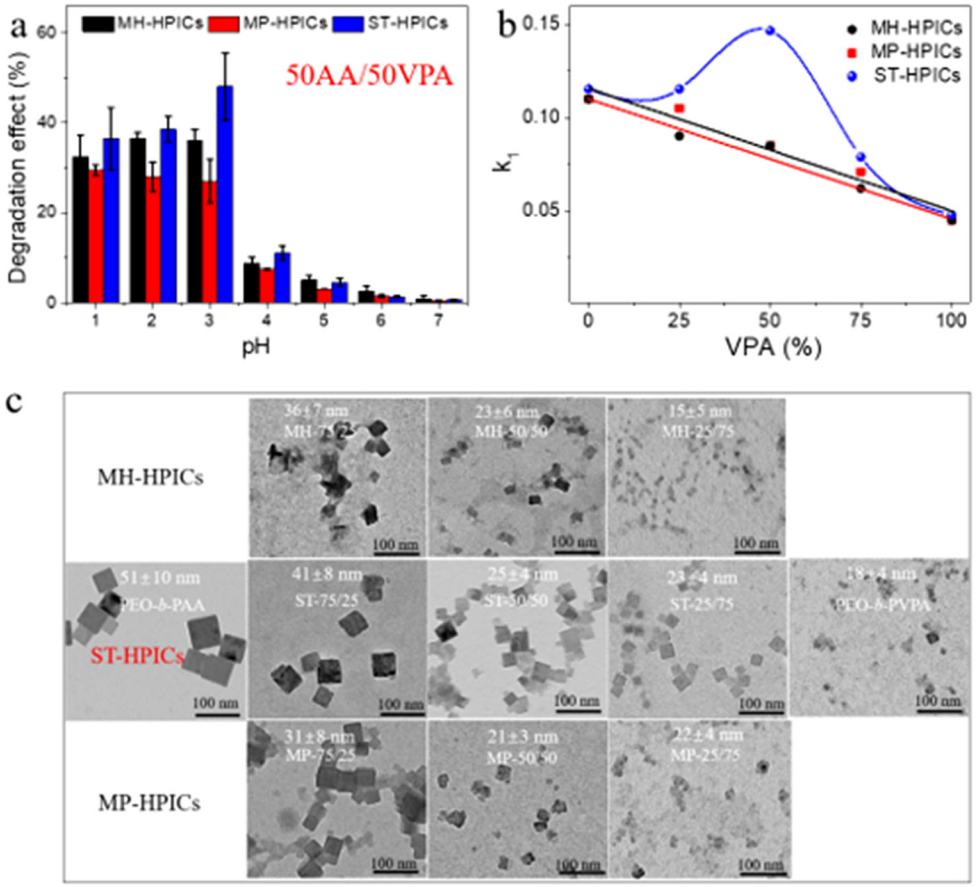

Fig. 4 Comparison of the properties of **ST-HPICs**, **MH-HPICs** and **MP-HPICs**. (a) Photo-Fenton degradation of AB1: conversion at different pHs for a constant 50/50 AA/VPA ratio. (b) Prussian blue formation: evolution of rate constants k_1 as a function of VPA content for the three families of colloidal structures. (c) TEM images of obtained PB nanoparticles (pH = 5).

addition, Prussian blue nanoparticles synthesized using **ST-HPICs** maintain a higher content of cubic structures compared to those synthesized using the other two methods (Fig. 4c and Fig. S10†).

The previously presented results strongly suggest a correlation between the AA/VPA ratio and various properties of HPICs. Instead of analyzing one by one such correlation, multivariate analysis methods were used in order to get a global statistical analysis of the previous data. Ten experimental data were selected, for all AA/VPA ratios and methods used to get such ratios: results related to the catalytic activity (degradation rate and amount of Fe(III) ions released at pH 1 and 3) or to the formation of Prussian blue nanoparticles (particle sizes obtained by TEM), fraction of cubic particles, maximum absorbance value after 2 hours, kinetic parameters of Prussian blue particle formation (k_1, k_2, and alpha) (Fig. 5). Correlation between the composition of the complexing block and the properties of HPICs is confirmed by calculating the two correlation matrices: the first is related to the catalytic properties of HPICs (Fig. 5a) and the second to the formation of Prussian blue nanoparticles (Fig. 5b). Particle size, cube proportion, kinetic constant k_1, pollutant degradation, and iron ion release at pH 1 and 3 are positively correlated with the proportion of AA, while the constants k_2 and alpha are negatively correlated. The high correlation coefficients (in absolute value) indicate that the overall composition in term of AA monomer is the primary factor controlling the properties of the final HPIC solutions. Again, this is understood in term of iron ions availability enhanced by AA *versus* VPA. These different experimental parameters are positively and significantly correlated with each other.

Principal component analysis (PCA) also highlights the predominant effect of the AA/VPA ratio. As seen in Fig. S11,† the two principal components, noted PC1 and PC2, enable to describe about 90% of the cumulative variance of the data. Fig. 5c and Fig. S11b† present the score plot issued from this PCA. The different systems are separated according to the main component PC1 based on photodegradation properties and the size of the particles obtained (see Fig. 5d). This separation reveals a strong correlation with the composition, with the points corresponding to a given composition mostly found in the same area of the graph. In addition, while samples with an AA/VPA composition of 75/25 are projected onto similar areas of the graph regardless of organization (**ST-HPICs**,

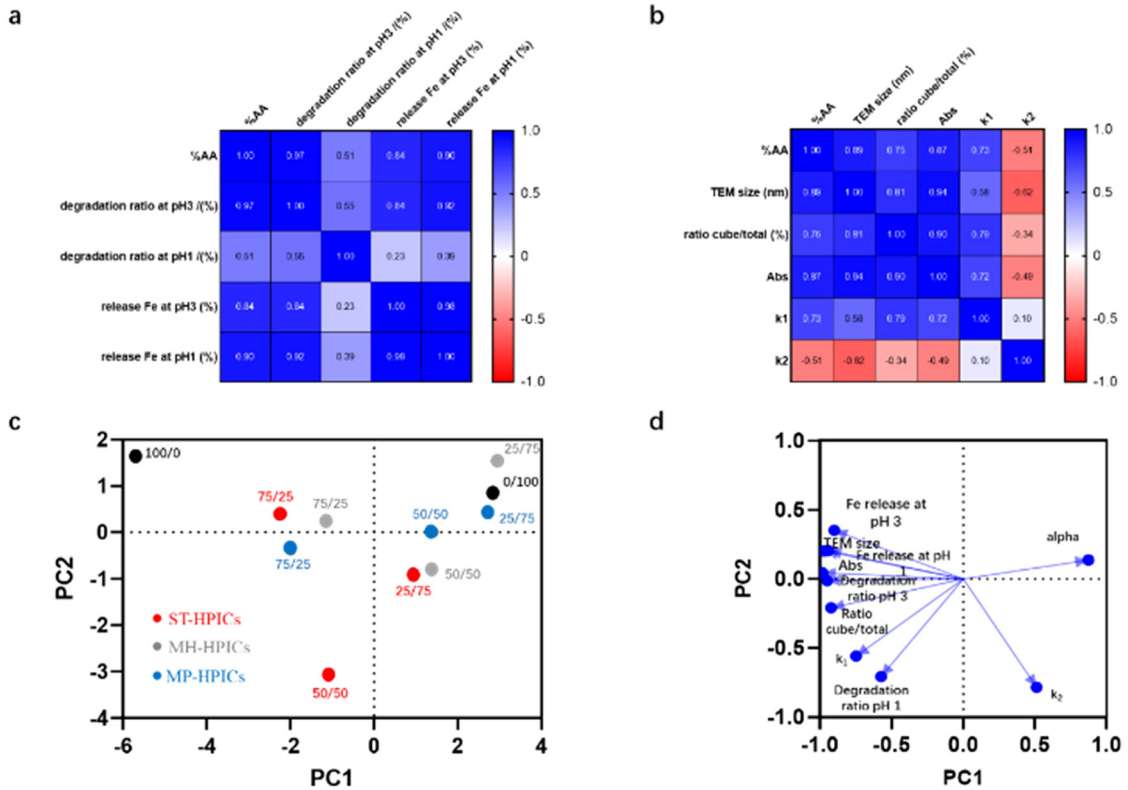

Fig. 5 Multivariate analysis of experimental data (see data in Table S2†). Correlation matrix between AA content and (a) catalysis data output (degradation of AB1 and release of Fe(III) ions at pH 1 an pH 3) and (b) Prussian blue formation output (TEM size ratio of cubic over the total amount of particle, value of the absorbance at the plateau after two hours, kinetic constant k_1, k_2). Principal component analysis (c) score plot and (d) corresponding loadings. PC1 is positively correlated with alpha and k_2 and negatively correlated with other studied variables; PC2 is negatively correlated with k_2, k_1, degradation ratio at pH 1 (see Fig. S11† for a complete description). PC1 and PC2 represent 89.2% of total variance.

MH-HPICs or **MP-HPICs**), this is not the case for projections corresponding to compositions of 50/50 and 25/75. This difference highlights the distinct properties of systems based on statistical copolymers, which, for a fixed composition, are distinguished by their ability to generate higher proportions of cubic particles and lead to different kinetic profiles (such as the value of alpha...). This can also be seen in less global analysis: plots of Prussian Blue nanoparticle sizes *versus* one other experimental parameter (see Fig. S12†) often present a large discrepancy between **ST-HPICs** and the other systems for AA/VPA ratio of 50/50. Therefore, one can conclude that the microstructure within the statistical AA/VPA copolymer is not always equivalent to a mixture of copolymers with pure AA or VPA blocks.

The second clear conclusion is that **MH-HPICs** and **MP-HPICs** are more or less equivalent. This is, for example, seen in Fig. 4a and b where the kinetic data of **MH-HPICs** and **MP-HPICs** are similar within experimental error. To understand such a result, one can suggest the hypothesis that polymers or iron ions exchange can occurs in these HPIC solutions.

To probe this, a series of NMR experiments was therefore conducted by adding increasing amounts of PEG-*b*-PVPA to a solution of HPICs made by PEG-*b*-PAA and gallium ions in the presence of methyl sulfone as internal standard (Fig. 6a). Gallium was chosen because of its ionicity equivalent to that of Fe(III) and to avoid the inherent paramagnetic effects of Fe (III). The evolution of NMR spectra is shown in Fig. 6b (see also Fig. S13†). While the hydrogen atoms (H) in alpha position to the carboxylic acid functions disappear after complexation with the HPICs-PAA system, the gradual addition of PEG-*b*-PVPA induces the progressive reappearance of the signal related to this polymer. If the evolution of the ratio of intensities between the H associated with carboxylates and those of the internal standard is plotted against the PEG-*b*-PVPA content (Fig. 6c), the calculated values correspond to a quantitative substitution of PEG-*b*-PAA. The evolution of the H's T_1 relaxation times confirms this hypothesis. The complexation of PEG-*b*-PAA by Ga^{3+} ions evidenced an average short T_1 of 790(±40) ms for the H in the 1.9–2.4 ppm area corresponding to H in alpha of the carboxylic and phosphonic acids in HPICs-PAA and -PVPA (Fig. 6d). Substitution by PEG-*b*-PVPA leads to a progressive increase in the measured T_1 up to 1040 (±40) ms reaching the one of HPICs-PVPA measured at 960 (±160) ms. Thus, adding a sufficient amount of PEG-*b*-PVPA to complex all the metal ions present in HPICs-PAA solutions results in the formation of HPICs-PVPA within a few hours.

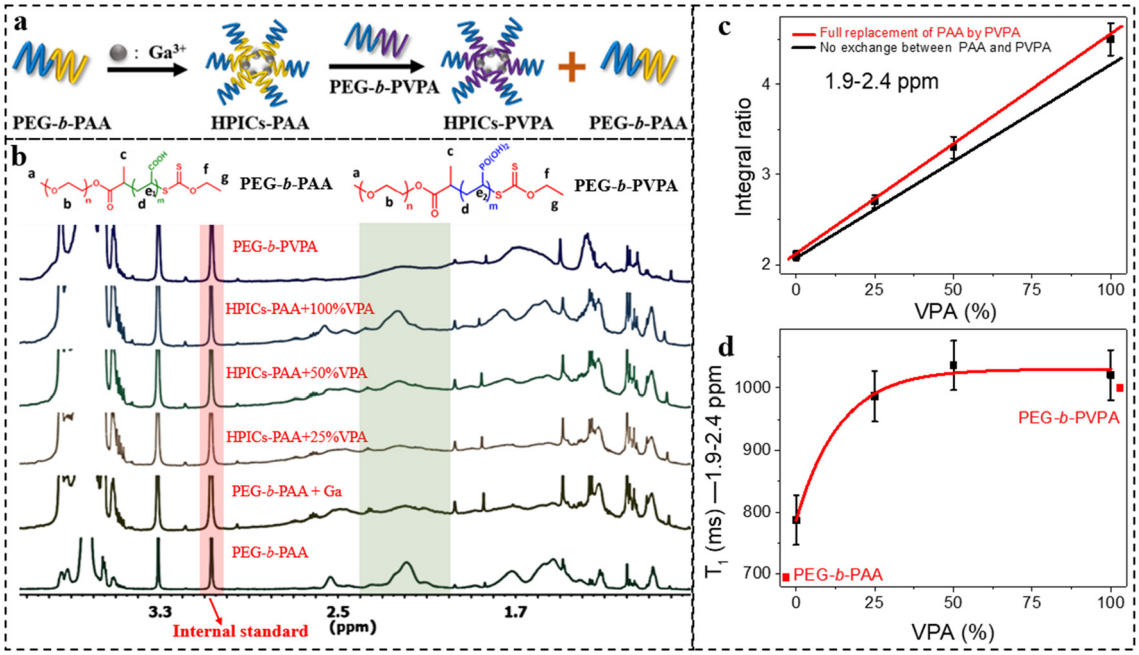

Fig. 6 (a) Schematic diagram of the NMR experiments to probe the exchange of PEG-*b*-PAA by PEG-*b*-PVPA in HPIC structures. (b) NMR spectra of mixtures containing HPICs-PAA and different amounts of PEG-*b*-PVPA added (see Fig. S13 for the signal assignment†). In grey, the domain related to H in alpha position to the carboxylic and phosphonic acids in PEG-*b*-PAA and -PVPA. (c) Evolution of the integral ratio of protons associated with carboxylate (phosphate, 1.9–2.4 ppm) units to internal standard units (methyl sulfone, ~3.0 ppm). Red line represents expected values of integral ratio assuming a full replacement of PEG-*b*-PAA by PEG-*b*-PVPA while black line assumed that such a replacement does not occur. (d) Evolution of T1 (1.9–2.4 ppm) with %VPA in the charged block.

Therefore, from these results, we can assume that polymers based on VPA could be exchanged with PEG-*b*-PAA in HPICs. The reverse is impossible or very difficult.

These NMR results, in addition to previous findings demonstrating strong similarities in properties between the two **MH-HPICs** and **MP-HPICs** systems and very rapid formation kinetics, suggest the possibility of exchanges within the HPIC structures, which could render the two **MH-HPICs** and **MP-HPICs** systems equivalent if a fast equilibrium and exchange occurred. However, further studies are required to confirm this hypothesis.

Conclusions

This study investigates the formation and properties of hybrid polyionic complexes (HPICs) derived from double hydrophilic block copolymers (DHBCs), focusing on the relationship between their composition and structure and resulting characteristics. For this, a series of anionic-neutral block copolymers with varying ratios of acrylic acid (AA) and vinylphosphonic acid (VPA) in the anionic block are synthesized and used to form HPICs in the presence of Fe(III) ions. Dynamic light scattering (DLS) analysis revealed that the addition of Fe(III) ions promoted the formation of monodisperse colloids, with their size and stability significantly influenced by the AA/VPA ratio. HPICs with higher VPA content exhibited better stability at low pH, suggesting stronger interactions between VPA and iron ions. The catalytic properties of these HPICs were assessed using a photo-Fenton process to degrade a model pollutant, naphthol blue black (AB1). Results indicated that HPICs with higher VPA content had reduced catalytic efficiency at higher pH levels, likely due to the strong binding of VPA units to iron ions, which altered the redox potential and hindered hydroxyl radical production. However, at lower pH, VPA improved the HPICs' stability and reactivity. Additionally, the ability of HPICs to act as reservoirs for Prussian blue nanoparticle formation was examined. Higher VPA content led to smaller, less defined nanoparticles with a decrease in the proportion of cubic particles. Kinetic analysis showed that HPICs with a 50/50 AA/VPA composition provided the best balance between stability and reactivity, resulting in faster reaction rates and more uniform nanoparticles. Lastly, beyond composition, HPIC solutions obtained using different formulation conditions of HPICs presenting different local organizations also present distinctive properties. In conclusion, the study demonstrates that both the composition and microstructure of DHBCs are crucial in determining the properties and performance of HPICs. By controlling these variables and conditions of formulation, it is possible to tailor HPICs through the modification of the coordination sphere of iron for specific applications such as catalysis or nanoparticle synthesis. These adjustments allow for precise control of the final properties of HPICs, thereby paving the way for numerous potential

applications in the fields of advanced materials, catalysis, and biotechnology.

Author contributions

Liming Peng: resources, experiments, investigation, writing – original draft, writing – review & editing. Maksym Odnoroh: resources, editing. Mathias Destarac: editing. Yannick Coppel: experiments, editing. Céline Delmas: analysing. Florence Benoît-Marquié: conceptualization, investigation, writing–original draft. Christophe Mingotaud: conceptualization, investigation, writing–original draft. Jean-Daniel Marty: funding acquisition, writing – original draft, writing – review & editing.

Data availability

The data supporting this article have been included as part of the ESI.†

Conflicts of interest

The authors declare that they have no known competing financial interests or personal relationships that could have appeared to influence the work reported in this paper.

Acknowledgements

The author thanks CNRS, University Paul Sabatier and the China Scholarship Council (CSC) for financial support. The authors extend their gratitude to Olivier Coutelier's help with polymer synthesis. The authors thank Dominique Goudenèche and Bruno Payre from the CMEAB platform for their assistance with TEM.

References

1 D. T. Gentekos, R. J. Sifri and B. P. Fors, *Nat. Rev. Mater.*, 2019, **4**, 761–774.
2 Y. Lu, T. Nemoto, M. Tosaka and S. Yamago, *Nat. Commun.*, 2017, **8**, 1863.
3 J.-F. Lutz, J.-M. Lehn, E. W. Meijer and K. Matyjaszewski, *Nat. Rev. Mater.*, 2016, **1**, 16024.
4 C. Piliego, T. W. Holcombe, J. D. Douglas, C. H. Woo, P. M. Beaujuge and J. M. Fréchet, *J. Am. Chem. Soc.*, 2010, **132**, 7595–7597.
5 J. M. Lee, J. Kwon, S. J. Lee, H. Jang, D. Kim, J. Song and K. T. Kim, *Sci. Adv.*, 2022, **8**, eabl8614.
6 J.-F. Lutz, M. Ouchi, D. R. Liu and M. Sawamoto, *Science*, 2013, **341**, 1238149.
7 D. Wang, Y. Jin, X. Zhu and D. Yan, *Prog. Polym. Sci.*, 2017, **64**, 114–153.
8 Y. Zheng, S. Li, Z. Weng and C. Gao, *Chem. Soc. Rev.*, 2015, **44**, 4091–4130.
9 Z. Zhang, P. Li, M. Xiong, L. Zhang, J. Chen, X. Lei, X. Pan, X. Wang, X.-Y. Deng, W. Shen, Z. Mei, K.-K. Liu, G. Liu, Z. Huang, S. Lv, Y. Shao and T. Lei, *Sci. Adv.*, 2024, **10**, eadk0647.
10 J. Zhuang, M. R. Gordon, J. Ventura and L. Li, *Chem. Soc. Rev.*, 2013, **42**, 7421–7435.
11 M. A. C. Stuart, W. T. S. Huck, J. Genzer, M. Müller, C. Ober, M. Stamm, G. B. Sukhorukov, I. Szleifer, V. V. Tsukruk, M. Urban, F. Winnik, S. Zauscher, I. Luzinov and S. Minko, *Nat. Mater.*, 2010, **9**, 101–113.
12 G. V. Jensen, R. Lund, J. Gummel, M. Monkenbusch, T. Narayanan and J. S. Pedersen, *J. Am. Chem. Soc.*, 2013, **135**, 7214–7222.
13 K. Schäfer, H. B. Kolli, M. Killingmoe Christensen, S. L. Bore, G. Diezemann, J. Gauss, G. Milano, R. Lund and M. Cascella, *Angew. Chem.*, 2020, **132**, 18750–18757.
14 K. Tse-Ve-Koon, N. Tremblay, D. Constantin and É. Freyssingeas, *J. Colloid Interface Sci.*, 2013, **393**, 161–173.
15 R. Haag and F. Kratz, *Angew. Chem., Int. Ed.*, 2006, **45**, 1198–1215.
16 H. Cabral, K. Miyata, K. Osada and K. Kataoka, *Chem. Rev.*, 2018, **118**, 6844–6892.
17 I. Dimitrov, B. Trzebicka, A. H. E. Müller, A. Dworak and C. B. Tsvetanov, *Prog. Polym. Sci.*, 2007, **32**, 1275–1343.
18 C. J. F. Rijcken, O. Soga, W. E. Hennink and C. F. V. Nostrum, *J. Controlled Release*, 2007, **120**, 131–148.
19 A. Nabiyan, J. B. Max and F. H. Schacher, *Chem. Soc. Rev.*, 2022, **51**, 995–1044.
20 A. El Jundi, S. J. Buwalda, Y. Bakkour, X. Garric and B. Nottelet, *Adv. Colloid Interface Sci.*, 2020, **283**, 102213.
21 S. Gineste and C. Mingotaud, *Adv. Colloid Interface Sci.*, 2023, **311**, 102808.
22 X. Li, J. Iocozzia, Y. Chen, S. Zhao, X. Cui, W. Wang, H. Yu, S. Lin and Z. Lin, *Angew. Chem., Int. Ed.*, 2018, **57**, 2046–2070.
23 A. Wibowo, K. Osada, H. Matsuda, Y. Anraku, H. Hirose, A. Kishimura and K. Kataoka, *Macromolecules*, 2014, **47**, 3086–3092.
24 J.-B. Masclef, J. Prunet and B. V. K. J. Schmidt, *Adv. Sci.*, 2024, **11**, 2310277.
25 F. H. Schacher, P. A. Rupar and I. Manners, *Angew. Chem., Int. Ed.*, 2012, **51**, 7898–7921.
26 Y. Wu, H. Hu, J. Hu, T. Liu, G. Zhang and S. Liu, *Langmuir*, 2013, **29**, 3711–3720.
27 J. Chen, B. Yan, X. Wang, Q. Huang, T. Thundat and H. Zeng, *Polym. Chem.*, 2017, **8**, 3066–3073.
28 G. Mountrichas and S. Pispas, *Macromolecules*, 2006, **39**, 4767–4774.
29 S. Jiang, Y. Yao, Y. Nie, J. Yang and J. Yang, *J. Colloid Interface Sci.*, 2011, **364**, 264–271.
30 A. Klaikherd, C. Nagamani and S. Thayumanavan, *J. Am. Chem. Soc.*, 2009, **131**, 4830–4838.
31 A. Sundararaman, T. Stephan and R. B. Grubbs, *J. Am. Chem. Soc.*, 2008, **130**, 12264–12265.

32 S. Gineste, E. Di Cola, B. Amouroux, U. Till, J.-D. Marty, A.-F. Mingotaud, C. Mingotaud, F. Violleau, D. Berti, G. Parigi, C. Luchinat, S. Balor, M. Sztucki and B. Lonetti, *Macromolecules*, 2018, **51**, 1427–1440.
33 K. Kataoka, A. Harada and Y. Nagasaki, *Adv. Drug Delivery Rev.*, 2012, **64**, 37–48.
34 M. Mestivier, J. R. Li, A. Camy, C. Frangville, C. Mingotaud, F. Benoît-Marquié and J.-D. Marty, *Chem. – Eur. J.*, 2020, **26**, 14152–14158.
35 L. Peng, C. Mingotaud, F. Benoît-Marquié and J.-D. Marty, *ACS Appl. Nano Mater.*, 2022, **5**, 11458–11464.
36 J.-M. Park, M.-H. Choi, E. Lee and S.-M. Lee, *ACS Appl. Polym. Mater.*, 2023, **5**, 7411–7419.
37 C. Frangville, Y. Li, C. Billotey, D. R. Talham, J. Taleb, P. Roux, J.-D. Marty and C. Mingotaud, *Nano Lett.*, 2016, **16**, 4069–4073.
38 M. Yon, S. Gineste, G. Parigi, B. Lonetti, L. Gibot, D. R. Talham, J.-D. Marty and C. Mingotaud, *ACS Appl. Nano Mater.*, 2021, **4**, 4974–4982.
39 S. Gineste, B. Lonetti, M. Yon, J. Giermanska, E. Di Cola, M. Sztucki, Y. Coppel, A.-F. Mingotaud, J.-P. Chapel, J.-D. Marty and C. Mingotaud, *J. Colloid Interface Sci.*, 2022, **609**, 698–706.
40 H.-W. Shin, H. Sohn, Y.-H. Jeong and S.-M. Lee, *Langmuir*, 2019, **35**, 6421–6428.
41 Y.-H. Jeong, H.-W. Shin, J.-Y. Kwon and S.-M. Lee, *ACS Appl. Mater. Interfaces*, 2018, **10**, 23617–23629.
42 W. Zhu, Y. Li, L. Liu, Y. Chen, C. Wang and F. Xi, *Biomacromolecules*, 2010, **11**, 3086–3092.
43 L. Peng, S. Gineste, C. Coudret, D. Ciuculescu-Pradines, F. Benoît-Marquié, C. Mingotaud and J.-D. Marty, *J. Colloid Interface Sci.*, 2023, **649**, 900–908.
44 E. Seo, J. Kim, Y. Hong, Y. S. Kim, D. Lee and B.-S. Kim, *J. Phys. Chem. C*, 2013, **117**, 11686–11693.
45 A. Witecka, J. Schmitt, M. Courtien, C. Gérardin and G. Rydzek, *Microporous Mesoporous Mater.*, 2024, **365**, 112913.
46 E. Seo, T. Lee, K. T. Lee, H.-K. Song and B.-S. Kim, *J. Mater. Chem.*, 2012, **22**, 11598–11604.
47 K. H. Markiewicz, L. Marmuse, M. Mounsamy, C. Billotey, M. Destarac, C. Mingotaud and J.-D. Marty, *ACS Macro Lett.*, 2022, **11**, 1319–1324.
48 M. Odnoroh, O. Coutelier, C. Mingotaud, M. Destarac and J.-D. Marty, *J. Colloid Interface Sci.*, 2023, **649**, 655–664.
49 M. Odnoroh, C. Mingotaud, O. Coutelier, J.-D. Marty and M. Destarac, *Eur. Polym. J.*, 2024, **210**, 112963.
50 C. C. Loures, M. A. Alcântara, H. J. I. Filho, A. Teixeira, F. T. Silva, T. C. Paiva and G. Samanamud, *Rev. Chem. Eng.*, 2013, **5**, 102–120.
51 A. Machulek Jr., J. E. F. Moraes, C. Vautier-Giongo, C. A. Silverio, L. C. Friedrich, C. A. O. Nascimento, M. C. Gonzalez and F. H. Quina, *Environ. Sci. Technol.*, 2007, **41**, 8459–8463.
52 P. Warneck, *Phys. Chem. Chem. Phys.*, 2018, **20**, 4020–4037.
53 A. Stefánsson, *Environ. Sci. Technol.*, 2007, **41**, 6117–6123.
54 J.-P. Simonin, *Chem. Eng. J.*, 2016, **300**, 254–263.
55 E. Neyens and J. Baeyens, *J. Hazard. Mater.*, 2003, **98**, 33–50.
56 M. T. Ball, J. Hay, H. M. Masrouji and J. K. Sugden, *Dyes Pigm.*, 1992, **19**, 51–57.